Tight-binding analysis of Si and GaAs ultrathin bodies with subatomic wave-function resolution

Yaohua P. Tan,[1,*] Michael Povolotskyi,[1] Tillmann Kubis,[1] Timothy B. Boykin,[2] and Gerhard Klimeck[1]

[1]*School of Electrical and Computer Engineering, Network for Computational Nanotechnology, Purdue University, West Lafayette, Indiana 47906, USA*

[2]*Department of Electrical and Computer Engineering, University of Alabama in Huntsville, Huntsville, Alabama 35899, USA*

(Received 12 March 2015; revised manuscript received 17 May 2015; published 4 August 2015)

Empirical tight-binding (ETB) methods are widely used in atomistic device simulations. Traditional ways of generating the ETB parameters rely on direct fitting to bulk experiments or theoretical electronic bands. However, ETB calculations based on existing parameters lead to unphysical results in ultrasmall structures like the As-terminated GaAs ultrathin bodies (UTBs). In this work, it is shown that more transferable ETB parameters with a short interaction range can be obtained by a process of mapping *ab initio* bands and wave functions to ETB models. This process enables the calibration of not only the ETB energy bands but also the ETB wave functions with corresponding *ab initio* calculations. Based on the mapping process, ETB models of Si and GaAs are parameterized with respect to hybrid functional calculations. Highly localized ETB basis functions are obtained. Both the ETB energy bands and wave functions with subatomic resolution of UTBs show good agreement with the corresponding hybrid functional calculations. The ETB methods can then be used to explain realistically extended devices in nonequilibrium that cannot be tackled with *ab initio* methods.

DOI: 10.1103/PhysRevB.92.085301 PACS number(s): 73.20.At, 73.61.Ey

I. INTRODUCTION

Modern semiconductor nanodevices have reached critical device dimensions in the sub-10-nm range. These devices comprise complicated two- or three-dimensional geometries and are composed of multiple materials. Confined geometries such as ultrathin bodies (UTBs) [1], Fin-Shaped Field Effect Transistor (FinFETs), [2] and nanowires [3] are usually adopted in nanometer-scale device designs to obtain desired performance characteristics. Most of the electrically conducting devices are not arranged in infinite periodic arrays but are of finite extent with contacts controlling the current injections and potential modulation. Typically, there are about 10 000 to 10×10^6 atoms in the active device region with contacts controlling the current injection. These finite-sized structures suggest an atomistic, local, and orbital-based electronic structure representation for device-level simulation. Quantitative device design requires reliable prediction of the materials' band gaps and band offsets within a few meV and important effective masses within a few percent in the geometrically confined active device regions. The empirical tight-binding (ETB) model is usually fitted to bulk dispersions without any definition of the spatial wave-function details. However, a recent *ab initio* study on UTBs [4] showed that the surface carrier distribution in confined systems is strongly geometry and material dependent. This suggests that the charge distribution for realistic predictions of nanodevice performances should be resolved with subatomic resolution.

Ab initio methods offer atomistic representations with subatomic resolution for a variety of materials. However, accurate *ab initio* methods, such as hybrid functionals [5] and GW [6] and Bethe–Salpeter Equation (BSE) approximations [7] are, in general, computationally too expensive to be applied to systems containing millions of atoms. Furthermore, those methods assume equilibrium and cannot truly model out-of-equilibrium device conditions where, e.g., a large voltage might have been applied to drive carriers. The ETB methods are numerically much more efficient than *ab initio* methods. For group IV and III–V semiconductors, an $sp^3d^5s^*$ ETB model with nearest-neighbor interactions is sufficient to model important valence and conduction valleys correctly. In the $sp^3d^5s^*$ ETB model, the basis set incorporates only ten orbitals (i.e. one s, three p, and five d orbitals and one excited s^* orbital) per atom. ETB has been established as the standard state-of-the-art basis for realistic device simulations [8]. It has been successfully applied to electronic structures of millions of atoms [9] as well as on nonequilibrium transport problems that even involve inelastic scattering [10]. The accuracy of the ETB methods depends critically on the careful calibration of the empirical parameters. The traditional way to determine the ETB parameters is to fit ETB band structures to experimental data of bulk materials [11,12].

The ETB basis functions remain implicitly defined during traditional fitting processes. The lack of explicit basis functions makes it difficult to predict wave-function-dependent quantities like optical matrix elements with high precision. More importantly, ETB models parameterized by traditional fitting processes suffer from potential ambiguity when applied to ultrasmall structures such as UTBs, nanowires, and more complicated geometries. For instance, the existing ETB parameters of GaAs [12] applied to an As-terminated GaAs UTB with an implicit hydrogen passivation model [13] results in unphysical top valence-band states as shown in Fig. 1: the real-space probability amplitudes of *ab initio* topmost valence bands correspond to confined states with the probability amplitude peaking in the center of the UTB rather than the surface of the UTB as in ETB. In Fig. 1, the hybrid functional calculations include hydrogen atoms explicitly, whereas the ETB calculations include only their impact implicitly [13]. The mismatch between the envelopes of ETB and *ab initio* wave functions suggests a calibration of wave functions in the ETB parametrization process is necessary. It is also found that the method of passivation (i.e., implicit or explicit

*tyhua02@gmail.com

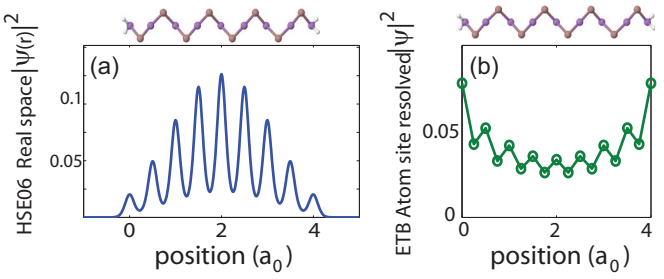

FIG. 1. (Color online) In As-terminated GaAs UTBs, (a) hybrid functional probability amplitudes of the top valence bands are confined states with probability amplitude peaking in the center of the UTB, while (b) the ETB valence states are surface states.

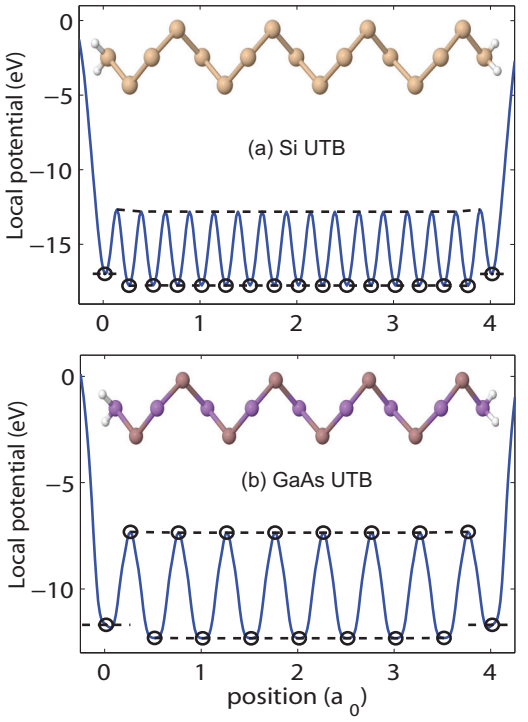

FIG. 2. (Color online) Planar averaged local potentials of hydrogen-terminated (a) Si and (b) GaAs UTBs. The dashed lines correspond to the envelopes of the local potentials; the dots on dashed lines correspond to centers of atoms. The envelopes of the potentials are flat inside the UTBs. Obvious deviation can be seen at the surface atoms.

inclusion of hydrogen atoms) has an effect on the nature of the valence-band states.

The ETB interaction range is an important concern when developing a transferable ETB model. Previous ETB studies on group III–V and IV materials [11,12] show that ETB models with first-nearest-neighbor interactions are adequate to model bulk group III–V and IV materials. In order to assess whether the ETB model with first-nearest-neighbor interactions can be transferred to nanostructures like UTBs, *ab initio* local potentials are studied. Here the *ab initio* calculations are based on projector-augmented-wave method (PAW) [14] formalism. The *ab initio* local potentials of Si and GaAs UTBs averaged over the transverse plane are shown in Fig. 2. It turns out that the envelopes of *ab initio* local potential are flat inside the UTBs. Obvious variation of the local potential can be observed only at the surface atoms. Local potential profiles similar to those in Fig. 2 have also been obtained by *ab initio* studies of transition-metal oxides [15] and graphene-metal interfaces [16]. This character in local potential suggests that hydrogen atoms mainly affect their first nearest neighbors, while the atoms inside the UTBs are weakly affected by hydrogen atoms. Therefore, longer-range interactions beyond first nearest neighbors are negligible, and the ETB models including only the first nearest neighbors are capable of modeling the UTB systems correctly.

Therefore, a more fundamental fitting process that relates both the band structure and the wave functions of ETB models with *ab initio* calculations is desirable to generate transferable ETB models. Existing approaches to construct localized basis functions and tight-binding-like Hamiltonians from *ab initio* results include maximally localized Wannier functions (MLWF) [17,18], quasiatomic orbitals [19,20], and density functional theory-tight binding (DFT-TB) analysis [21]. The MLWFs are constructed using Bloch states of either isolated bands [17] or entangled bands [18]. These methods typically include interatomic interactions beyond first nearest neighbors. However, these methods do not eliminate the above-discussed ambiguity of the commonly used orthogonal $sp^3d^5s^*$ ETB models with first-nearest-neighbor interactions. Furthermore, these approaches usually disregard excited orbitals (i.e., s^* and d orbitals for diamond and zinc-blende semiconductors), which are often needed to correctly parametrize conduction bands of semiconductors. Previous work already suggested how to generate ETB parameters that are compatible with typical ETB models and still reproduce *ab initio* results [22]. This previous method was already applied to several materials such as GaAs, MgO [22], and SmSe [23] and yielded good agreement between bulk ETB and *ab initio* band structures. However, the resulting wave functions did not satisfactorily agree with the *ab initio* wave functions.

In this paper, a parametrization algorithm is presented that "maps" *ab initio* results (i.e., eigenenergies and eigenfunctions) to tight-binding models. Compared with the previous work [22], the presented method allows much better agreement of the ETB and *ab initio* wave functions. In this present mapping algorithm, wave-function-derived ETB parameters for the Hamiltonian, for highly localized basis functions, and for explicit surface passivation are obtained. It is important to mention that the ETB Hamiltonian of this method can be limited to first-nearest-neighbor interactions. The mapping process is applied to both bulk Si and GaAs to generate ETB parameters and explicit basis functions from corresponding hybrid functional calculations. It is demonstrated in this work that the wave-function-derived ETB Hamiltonian does not yield the ambiguity discussed in relation to Fig. 1. In the same way, the transferability of the ETB model to nanostructures is improved. This is demonstrated by a comparison of ETB and hybrid functional results in GaAs and Si UTBs.

This paper is organized as follows. In Sec. II, the algorithm of parameter mapping from *ab initio* calculations to tight-binding models is described. Section III shows the application of the mapping algorithm to bulk and UTB

systems. Section III A presents the application of the present algorithm to bulk Si and GaAs. Bulk band structures and real-space basis functions are shown and discussed there as well. Section III B shows the application of the algorithm to UTB systems and compares ETB band structures and wave functions with corresponding *ab initio* results. The algorithm and its results are summarized in Sec. IV.

II. METHOD: PARAMETER-MAPPING ALGORITHM

The algorithm of the parameter mapping from *ab initio* results to ETB models is shown in Fig. 3. As will be shown in the following, the ETB parameters and basis functions are obtained in an iterative fitting procedure that spans over five steps (with steps 3 and 4 being iterated). The resulting first-nearest-neighbor Hamiltonian $\hat{H}^{TB}(\mathbf{k})$ is of the Slater-Koster table type [24,25]. The resulting basis $\mathfrak{B}_{\text{final}}$ is composed of orthonormal real-space functions $\mathfrak{B}_{\text{final}} = \{\Psi^{\text{final}}_{n,l,m}(\mathbf{r})\}$ which have the shape (vectors are given in bold type)

$$\Psi_{a,n,l,m}(\mathbf{r}) = \bar{Y}_{l,m}(\theta,\phi)\bar{R}_{a,n,l}(r) + \sum_{\substack{l',m' \\ (l',m') \neq (l,m)}} \bar{Y}_{l',m'}(\theta,\phi)\tilde{R}_{a,n,l,l',m'}(r). \quad (1)$$

Here a labels the atom type, whereas n, l, and m are principle, angular, and magnetic quantum numbers, respectively. All materials considered in this work contain no magnetic polarization. Therefore, the basis functions are spin independent. The tesseral spherical harmonics $\bar{Y}_{l,m}(\theta,\phi)$ describe the dependence of the basis functions on the angular coordinates θ and ϕ. The functions $\bar{R}_{a,n,l}(r)$ and $\tilde{R}_{a,n,l,l',m'}(r)$ define the radial r dependence of the basis functions. The contribution of $\tilde{R}_{a,n,l,l',m'}$ to the basis functions is much smaller than the contribution of $\bar{R}_{a,n,l}$. The detailed shapes of the radial functions $\bar{R}_{a,n,l}(r)$ and $\tilde{R}_{a,n,l,l',m'}(r)$ are subject to the fitting algorithm.

Step 1. First, electronic band structures $\varepsilon^{Ab}_j(\mathbf{k})$ and wave functions $\psi^{Ab}_{j,\mathbf{k}}$ are solved which serve as fitting targets to the overall mapping algorithm

$$\hat{H}^{Ab}(\mathbf{k})\left|\psi^{Ab}_{j,\mathbf{k}}\right\rangle = \varepsilon^{Ab}_j(\mathbf{k})\left|\psi^{Ab}_{j,\mathbf{k}}\right\rangle. \quad (2)$$

The index j corresponds to the band index, and $\mathbf{k}$ represents a momentum vector in the first Brillouin zone. In principle, any method that is capable of solving band diagrams and explicit basis functions can provide these fitting targets. Throughout this work, however, hybrid functional calculations are performed for step 1 [26].

Step 2. In the second step, initial guesses for the ETB basis functions and ETB parameters are defined. During the fitting process, the ETB basis $\mathfrak{B}_{\text{initial}}$ is spanned by nonorthogonal functions $\{\Phi_{a,n,l,m}(\mathbf{r})\}$ given by

$$\Phi_{a,n,l,m}(\mathbf{r}) = \bar{Y}_{l,m}(\theta,\phi)R_{a,n,l}(r). \quad (3)$$

$R_{a,n,l}(r)$ in Eq. (3) differ from $\bar{R}_{a,n,l}(r)$ of the final basis functions in Eq. (1). The ETB parameters and the parameters of the radial ETB basis functions $R_{a,n,l}(r)$ are adjusted iteratively in steps 3 and 4.

The details of the initial guesses for the diagonal and off-diagonal elements of the Hamiltonian $\hat{H}^{TB}(\mathbf{k})$ are not essential for the overall algorithm. Nevertheless, initial guesses that follow the framework of existing ETB parameter sets improve the overall fitting convergence. Urban *et al.* and Lu *et al.* discuss that interactions up to third nearest neighbors might be needed to exactly reproduce *ab initio* results [20,21]. In contrast, we find that the interatomic interaction elements of $\hat{H}^{TB}(\mathbf{k})$ can be limited to first-nearest-neighbor interactions throughout this work while still reproducing *ab initio* results very well.

Step 3. The nonorthogonal basis functions $\Phi_{a,n,l,m}(\mathbf{r})$ in position space are transformed into the Bloch representation [27] $\Phi_{a,n,l,m,\mathbf{k}}(\mathbf{r})$,

$$|\Phi_{\alpha,\mathbf{k}}\rangle \equiv \Phi_{a,n,l,m,\mathbf{k}}(\mathbf{r}) = \sum_{\mathbf{R}} \exp[i\mathbf{k}\cdot(\mathbf{R}+\boldsymbol{\tau}_a)]\Phi_{a,n,l,m}(\mathbf{r}-\mathbf{R}-\boldsymbol{\tau}_a), \quad (4)$$

where τ_a is the position of atom type a in the unit cell and the sum runs over all unit cells of the system with $\mathbf{R}$, the position of the respective cell. To improve readability of all formulas in the Dirac notation, the indices of atom type and quantum numbers are merged into Greek indices $\alpha = (a,n,l,m)$. For the remaining steps, an orthogonal basis $\mathfrak{B}_{\text{ortho}} = \{|\Psi_{\alpha,\mathbf{k}}\rangle\}$ is created out of the basis $\mathfrak{B}_{\text{initial}}$ with Löwdin's symmetrical orthogonalization algorithm [28]. Since steps 4 and 5 are formulated in the basis $\mathfrak{B}_{\text{ortho}}$, the wave functions $|\psi^{Ab}_{j,\mathbf{k}}\rangle$ of step 1 must be transformed into this basis,

$$\left|\psi^{Ab}_{j,\mathbf{k}}\right\rangle \approx \hat{P}(\mathbf{k})\left|\psi^{Ab}_{j,\mathbf{k}}\right\rangle = \sum_{\alpha} c_{j,\alpha}(\mathbf{k})|\Psi_{\alpha,\mathbf{k}}\rangle, \quad (5)$$

where

$$c_{j,\alpha}(\mathbf{k}) = \left\langle\Psi_{\alpha,\mathbf{k}}\middle|\psi^{Ab}_{j,\mathbf{k}}\right\rangle, \quad (6)$$

$c_{j,\alpha}(\mathbf{k}) = \langle\Psi_{\alpha,\mathbf{k}}|\psi^{Ab}_{j,\mathbf{k}}\rangle$, with the projection operator

$$\hat{P}(\mathbf{k}) = \sum_{\alpha} |\Psi_{\alpha,\mathbf{k}}\rangle\langle\Psi_{\alpha,\mathbf{k}}|. \quad (7)$$

Equation (5) contains an approximation of the *ab initio* wave functions in so far as the sum over α extends only over those

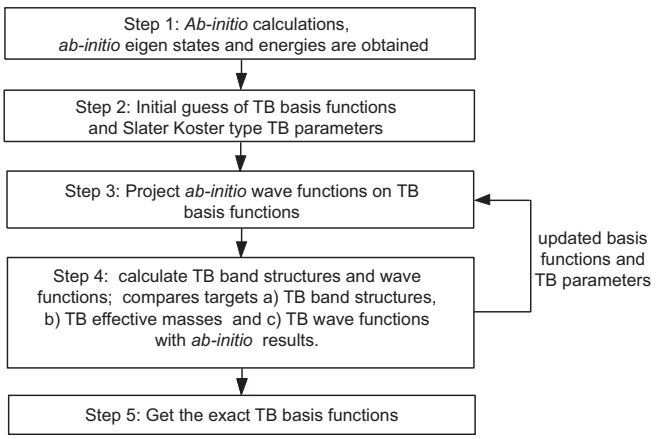

FIG. 3. The process of mapping from *ab initio* calculations to tight binding by which the ETB parameters and ETB basis functions are extracted iteratively.

orbitals that are included in the tight-binding basis $\mathfrak{B}_{\text{ortho}}$. This basis and $\mathfrak{B}_{\text{ortho}}$ from similar ETB models have many fewer basis vectors than the input *ab initio* calculation. This rank reduction is a typical outcome of rectangular transformations such as $\hat{P}$ and is well known in the field of low-rank approximations [29].

Step 4. Here the quality of the ETB fitting is assessed. In this step, the band structures of the current ETB model $\varepsilon_j^{TB}(\mathbf{k})$ and the *ab initio* input $\varepsilon_j^{Ab}(\mathbf{k})$ are compared. If these sufficiently agree, the phases of the ETB wave functions are modulated to agree with the *ab initio* ones, and both wave functions are compared after that. The ETB Hamiltonian from step 2 is diagonalized in the basis $\mathfrak{B}_{\text{ortho}}$ from step 3 to obtain ETB band structures $\varepsilon_j^{TB}(\mathbf{k})$ and eigenvectors $|\psi_{j,\mathbf{k}}^{TB}\rangle$,

$$\hat{H}^{TB}(\mathbf{k})\big|\psi_{j,\mathbf{k}}^{TB}\big\rangle = \varepsilon_j^{TB}(\mathbf{k})\big|\psi_{j,\mathbf{k}}^{TB}\big\rangle, \tag{8}$$

with

$$\big|\psi_{j,\mathbf{k}}^{TB}\big\rangle = \sum_{\alpha} d_{j,\alpha}(\mathbf{k})|\Psi_{\alpha,\mathbf{k}}\rangle. \tag{9}$$

To assess the quality of the ETB results, different fitness functions F_ε, F_m, and F_ψ are defined for energies, masses, and wave functions, respectively. F_ε and F_m are given by

$$F_\varepsilon = \sum_{j,\mathbf{k}} w_j^{\varepsilon}(\mathbf{k})\big|\varepsilon_j^{TB}(\mathbf{k}) - \varepsilon_j^{Ab}(\mathbf{k})\big|^2, \tag{10}$$

$$F_m = \sum_{m} w_m \left|\frac{m^{Ab} - m^{TB}}{m^{Ab}}\right|^2, \tag{11}$$

where $w_j^{\varepsilon}(\mathbf{k})$ and w_m are weights defined for each target.

As a convention for wave-function phases, another set of ETB wave functions $|\tilde{\psi}_{j,\mathbf{k}}^{TB}\rangle$ is introduced,

$$\big|\tilde{\psi}_{j,\mathbf{k}}^{TB}\big\rangle = \sum_{i} V_{j,i}(\mathbf{k})\big|\psi_{i,\mathbf{k}}^{TB}\big\rangle. \tag{12}$$

The unitary transformation $\hat{V}(\mathbf{k})$ is defined by

$$V_{j,i}(\mathbf{k}) = \frac{\big\langle\psi_{j,\mathbf{k}}^{TB}\big|\psi_{i,\mathbf{k}}^{Ab}\big\rangle}{\lambda(\mathbf{k})}, \tag{13}$$

with

$$\lambda(\mathbf{k}) = \sqrt{\frac{1}{N}\sum_{q,p}\big|\big\langle\psi_{q,\mathbf{k}}^{Ab}\big|\psi_{p,\mathbf{k}}^{TB}\big\rangle\big|^2}. \tag{14}$$

Here the sum over p and q runs over all N ETB states $|\psi_{p,\mathbf{k}}^{TB}\rangle$ and N *ab initio* states $\langle\psi_{q,\mathbf{k}}^{Ab}|$ with equivalent energies $\varepsilon_p^{TB}(\mathbf{k}) \approx \varepsilon_q^{Ab}(\mathbf{k})$. With this transformation, the equation

$$\big\langle\psi_{i,\mathbf{k}}^{Ab}\big|\tilde{\psi}_{j,\mathbf{k}}^{TB}\big\rangle = \lambda(\mathbf{k}) \tag{15}$$

holds for equivalent states. This phase adaption can only work if the ETB band structure is close enough to the *ab initio* result. The ETB wave-function fitness is given by

$$F_\psi = \sum_{j,\mathbf{k}} w_j^{\psi}(\mathbf{k})\big\|\big|\psi_{j,\mathbf{k}}^{Ab}\big\rangle - \big|\tilde{\psi}_{j,\mathbf{k}}^{TB}\big\rangle\big\|^2. \tag{16}$$

The weights $w_j^{\psi}(\mathbf{k})$ vary depending on the respective fitting focuses. Deviations of $|\tilde{\psi}_{\nu,\mathbf{k}}^{TB}\rangle$ from $|\psi_{\nu,\mathbf{k}}^{Ab}\rangle$ have, in general, two causes: inadequate basis functions and/or eigenfunctions of a poorly approximated ETB Hamiltonian. Therefore, F_ψ can be estimated as

$$\begin{aligned}\big\|\big|\psi_{j,\mathbf{k}}^{Ab}\big\rangle - \big|\tilde{\psi}_{j,\mathbf{k}}^{TB}\big\rangle\big\|^2 \leqslant\ & 2\big\|[\hat{I} - \hat{P}(\mathbf{k})]\big|\psi_{j,\mathbf{k}}^{Ab}\big\rangle\big\|^2 \\ & + 2\big\|\hat{P}(\mathbf{k})\big|\psi_{j,\mathbf{k}}^{Ab}\big\rangle - \big|\tilde{\psi}_{j,\mathbf{k}}^{TB}\big\rangle\big\|^2.\end{aligned} \tag{17}$$

The first term on the right-hand side of the last equation describes the deviation of the low-rank approximated *ab initio* wave functions. This becomes obvious with the projector property $\hat{P}^2(\mathbf{k}) = \hat{P}(\mathbf{k})$,

$$\big\|[\hat{I} - \hat{P}(\mathbf{k})]\big|\psi_{j,\mathbf{k}}^{Ab}\big\rangle\big\|^2 = \big\langle\psi_{j,\mathbf{k}}^{Ab}\big|[\hat{I} - \hat{P}(\mathbf{k})]\big|\psi_{j,\mathbf{k}}^{Ab}\big\rangle. \tag{18}$$

The second term on the right-hand side of Eq. (17) contains information about the quality of the eigenfunctions of the approximate ETB Hamiltonian $\hat{H}^{TB}(\mathbf{k})$. This is understandable when Eqs. (5) and (12) are inserted into this term,

$$\begin{aligned}&\big\|\hat{P}(\mathbf{k})\big|\psi_{j,\mathbf{k}}^{Ab}\big\rangle - \big|\tilde{\psi}_{j,\mathbf{k}}^{TB}\big\rangle\big\|^2 \\ &\quad = 2 - 2\,\mathrm{Re}\left[\sum_{\alpha,i} c_{j,\alpha}^{\dagger}(\mathbf{k})V_{j,i}(\mathbf{k})d_{i,\alpha}(\mathbf{k})\right].\end{aligned} \tag{19}$$

The fitness function F_ψ represents a major improvement over the traditional ETB eigenvalue fitting (e.g., typically limited to energies and effective masses). All fitness functions are minimized by iterating over steps 3 and 4: the Slater-Koster-type parameters for the ETB Hamiltonian $\hat{H}^{TB}(\mathbf{k})$ and the parameters of the radial ETB basis functions $R_{a,n,l}(r)$ are adjusted for every iteration of step 3.

Step 5. Once the fitness functions are small enough to end the iterations, it is assumed that those eigenfunctions of the ETB Hamiltonian $\hat{H}^{TB}(\mathbf{k})$ that were subject to the fitting are identical to the eigenfunctions of the *ab initio* Hamiltonian $\hat{H}^{Ab}(\mathbf{k})$ after a transformation $\hat{A}(\mathbf{k})$,

$$\big|\psi_{j,\mathbf{k}}^{TB}\big\rangle \approx \sum_{i} A_{j,i}(\mathbf{k})\big|\psi_{i,\mathbf{k}}^{Ab}\big\rangle. \tag{20}$$

This transformation $\hat{A}$ is determined by a singular-value decomposition of the rectangular overlap matrix of *ab initio* eigenstates with ETB eigenstates,

$$\big\langle\psi_{i,\mathbf{k}}^{Ab}\big|\psi_{j,\mathbf{k}}^{TB}\big\rangle = \sum_{p} U_{i,p}(\mathbf{k})\Sigma_{p,p}(\mathbf{k})W_{p,j}(\mathbf{k}). \tag{21}$$

The row index i runs over all *ab initio* eigenstates, exceeding those that served as fitting targets, whereas the column index j covers all the ETB eigenfunctions. Σ and W are square matrices, and U is a rectangular matrix. The transformation $\hat{A}$ is then defined as

$$A_{j,i}(\mathbf{k}) = \sum_{p} W_{j,p}(\mathbf{k})U_{p,i}^{\dagger}(\mathbf{k}). \tag{22}$$

$\hat{A}$ is constructed from relevant columns of a unitary transformation. Combining Eqs. (20) and (9) allows us to determine the Bloch periodic final basis functions,

$$\big|\Psi_{\alpha,\mathbf{k}}^{\text{final}}\big\rangle = \sum_{i,j} d_{\alpha,j}^{\dagger}(\mathbf{k})A_{j,i}(\mathbf{k})\big|\psi_{i,\mathbf{k}}^{Ab}\big\rangle. \tag{23}$$

The real-space counterpart of $|\Psi_{\alpha,\mathbf{k}}^{\text{final}}\rangle$ is given by

$$\Psi_{\alpha}^{\text{final}}(\mathbf{r} - \mathbf{R} - \tau) = \frac{V}{(2\pi)^3}\int_{\text{BZ}} d\mathbf{k}e^{-i\mathbf{k}\cdot(\mathbf{R}+\tau)}\Psi_{\alpha,\mathbf{k}}^{\text{final}}(\mathbf{r}). \tag{24}$$

III. RESULTS

In this work, *ab initio* level calculations of Si and GaAs systems were performed with VASP [30]. The screened hybrid functional of Heyd, Scuseria, and Ernzerhof (HSE06) [31] is used to produce band gaps [26] comparable with experiments in both the bulk and the UTB cases. In the HSE06 hybrid functional method, the total exchange energy incorporates 25% short-range Hartree-Fock (HF) exchange and 75% Perdew-Burke-Ernzerhof (PBE) exchange [32]. The screening parameter μ which defines the range separation is empirically set to 0.2 Å for both the HF and PBE parts. The correlation energy is described by the PBE functional. In all presented HSE06 calculations, a cutoff energy of 350 eV is used. Γ-point centered Monkhorst-Pack k-space grids are used for both bulk and UTB systems. The size of the k-space grid for bulk calculations is $6 \times 6 \times 6$, while the one for UTB is $6 \times 6 \times 1$. k points with integration weights equal to zero are added to the original $6 \times 6 \times 6$ or $6 \times 6 \times 1$ grid in order to generate energy bands with higher k-space resolution. PAW [14] pseudopotentials are used in all HSE06 calculations. The pseudopotentials for Si, Ga, and As atoms include the outermost occupied s and p atomic states as valence states. The low-lying $3d$ states of Ga are treated as core states since the incorporation of $3d$ states as valence states leads to less than 1% changes to fitting targets shown in Tables I and II for bulk materials. The spin-orbit coupling is included in band structure calculations. Small hydrostatic strains up to 0.3% are introduced to adjust the bulk band gaps in order to match experimental results. The lattice constant used in this work is given by Table III.

A. Application to bulk materials

For bulk Si and GaAs, fitting targets include the band structures of the lowest 16 bands (with spin degeneracy) along high-symmetry directions, important effective masses, and wave functions at high-symmetry points such as Γ, L, and X points. ETB basis functions in real space are reconstructed on the $6 \times 6 \times 6$ Γ center k-space grid using Eq. (24).

TABLE I. Comparison of targets' bulk Si. Critical band edges and effective masses at Γ, X, and L points from ETB and HSE06 calculations are compared. E_g and Δ_{SO} are in eV; effective masses are scaled by free-electron mass m_0. The error column summarizes the discrepancies between the HSE06 and TB results.

	Si			
Targets	TB Ref	HSE06	TB	Error (%)
$E_g(\Gamma)$	3.399	3.302	3.244	1.8
$E_g(X)$	1.131	1.142	1.139	0.2
$E_g(L)$	2.383	2.247	2.188	2.6
Δ_{SO}	0.047	0.051	0.052	0.8
m_{hh100}	0.299	0.281	0.282	0.097
m_{hh110}	0.633	0.566	0.572	0.977
m_{hh111}	0.796	0.704	0.714	1.433
m_{lh100}	0.232	0.206	0.204	1.001
m_{lh110}	0.165	0.151	0.149	0.937
m_{lh111}	0.156	0.143	0.142	0.927
m_{so100}	0.266	0.244	0.242	0.809
m_{so110}	0.266	0.244	0.242	0.795
m_{so111}	0.267	0.244	0.242	0.770
m_{cXl}	0.887	0.928	0.857	7.615
m_{cXt}	0.225	0.207	0.215	3.544

TABLE II. Comparison of targets' bulk GaAs. Critical band edges and effective masses at Γ, X, and L from TB and HSE06 calculations are compared. E_g and Δ_{SO} are in eV; effective masses are scaled by free-electron mass m_0. The error column summarizes the discrepancies between HSE06 and TB results.

	GaAs			
Targets	TB Ref	HSE06	TB	Error (%)
$E_g(\Gamma)$	1.424	1.418	1.416	0.2
$E_g(X)$	1.900	1.919	1.910	0.5
$E_g(L)$	1.707	1.702	1.708	0.3
Δ_{SO}	0.326	0.368	0.367	0.1
m_{hh100}	0.383	0.310	0.337	8.510
m_{hh110}	0.667	0.573	0.619	7.879
m_{hh111}	0.853	0.750	0.813	8.507
m_{lh100}	0.085	0.082	0.083	0.744
m_{lh110}	0.078	0.073	0.074	1.614
m_{lh111}	0.076	0.071	0.072	1.715
m_{so100}	0.166	0.164	0.160	1.998
m_{so110}	0.166	0.164	0.160	2.037
m_{so111}	0.166	0.164	0.160	2.041
m_{c100}	0.068	0.065	0.067	2.787
m_{c110}	0.068	0.066	0.067	2.790
m_{c111}	0.068	0.065	0.067	2.781
m_{cXl}	1.526	1.577	1.480	6.142
m_{cXt}	0.177	0.215	0.204	5.083
m_{cLl}	1.743	1.626	1.446	11.055
m_{cLt}	0.099	0.111	0.136	22.614

The band structures and density of states (DOS) of bulk Si and GaAs (HSE06 vs ETB) are shown in Figs. 4 and 5, respectively. The band structures using existing Si and GaAs ETB parameters [12,33] are also shown in corresponding figures. The ETB band structures and DOS using parameters generated from this work show better agreement with the corresponding hybrid functional results compared with the existing parameterizations. For bulk Si, the existing parametrization shows an unexpected low s^* band around 5 eV above the topmost valence bands. In the traditional fitting process, the s^* band shows a strong preference for moving downward [33]. Due to the large number of parameters to be determined, traditional (energy-gap and effective-mass) fitting procedures can find local minima in their fitness functions corresponding to wave functions significantly different from those predicted by *ab initio* methods. The present method has the important advantage that optimization involves not only masses and gaps but also wave functions. Thus, the ETB wave functions can be kept close to their *ab initio* counterparts. For GaAs, the existing parameterization shows 2 eV higher s-type low-lying valence bands. The ETB parameters of bulk Si and GaAs are listed in Table III. It can be seen from Tables I and II that the anisotropic hole masses from ETB show remarkable agreement with HSE06 results. The principal authors of the previous works [12,33] explicitly pointed out that fitting hole masses had been very difficult with the previous methods.

TABLE III. Slater-Koster-type ETB parameters of bulk Si and GaAs and passivation parameters of UTBs. All presented parameters except for the lattice constants are eV. The lattice constants are in angstroms. The hydrogen atoms which passivate As and Ga at surfaces are denoted by H_a and H_c, respectively. On-site energies of As and Ga at surfaces are shifted by δ_a and δ_c, respectively.

Si		GaAs			
a_0	5.43 Å	a_0	5.6307 Å		
E_s	−2.803316	E_{s_a}	−8.063758	E_{s_c}	−1.603222
E_p	4.096984	E_{p_a}	3.126841	E_{p_c}	4.745896
E_{s^*}	25.163115	$E_{s_a^*}$	21.930865	$E_{s_c^*}$	23.630466
E_d	12.568228	E_{d_a}	13.140998	E_{d_c}	14.807586
Δ	0.021926	Δ_a	0.194174	Δ_c	0.036594
$V_{ss\sigma}$	−2.066560	$V_{s_a s_c\sigma}$	−1.798514		
$V_{s^*s^*\sigma}$	−4.733506	$V_{s_a^* s_c^*\sigma}$	−4.112848		
$V_{ss^*\sigma}$	−1.703630	$V_{s_a s_c^*\sigma}$	−1.258382	$V_{s_c s_a^*\sigma}$	−1.688128
$V_{sp\sigma}$	3.144266	$V_{s_a p_c\sigma}$	3.116745	$V_{s_c p_a\sigma}$	2.776805
$V_{s^*p\sigma}$	2.928749	$V_{s_a^* p_c\sigma}$	1.635158	$V_{s_c^* p_a\sigma}$	3.381868
$V_{sd\sigma}$	−2.131451	$V_{s_a d_c\sigma}$	−0.396407	$V_{s_c d_a\sigma}$	−2.151852
$V_{s^*d\sigma}$	−0.176671	$V_{s_a^* d_c\sigma}$	−0.145161	$V_{s_c^* d_a\sigma}$	−0.810997
$V_{pp\sigma}$	4.122363	$V_{p_a p_c\sigma}$	4.034685		
$V_{pp\pi}$	−1.522175	$V_{p_a p_c\pi}$	−1.275446		
$V_{pd\sigma}$	−1.127068	$V_{p_a d_c\sigma}$	−1.478036	$V_{p_c d_a\sigma}$	−0.064809
$V_{pd\pi}$	2.383978	$V_{p_a d_c\pi}$	1.830852	$V_{p_c d_a\pi}$	2.829426
$V_{dd\sigma}$	−1.408578	$V_{d_a d_c\sigma}$	−1.216390		
$V_{dd\pi}$	2.284472	$V_{d_a d_c\pi}$	2.042009		
$V_{dd\delta}$	−1.541821	$V_{d_a d_c\delta}$	−1.829113		
H_{Si}		H_a(passivate As) and H_c(passivate Ga)			
E_{s_H}	−3.056510	$E_{s_{H_a}}$	2.758428	$E_{s_{H_c}}$	−0.308397
$V_{s_H s_{Si}\sigma}$	−4.859509	$V_{s_{H_a} s_a\sigma}$	−2.960420	$V_{s_{H_c} s_c\sigma}$	−3.151427
$V_{s_H p_{Si}\sigma}$	3.776178	$V_{s_{H_a} p_a\sigma}$	5.490764	$V_{s_{H_c} p_c\sigma}$	3.539284
$V_{s_H s_{Si}^*\sigma}$	0.0	$V_{s_{H_a} s_a^*\sigma}$	0.0	$V_{s_{H_c} s_c^*\sigma}$	−0.129904
$V_{s_H d_{Si}\sigma}$	−0.007703	$V_{s_{H_a} d_a\sigma}$	−1.727690	$V_{s_{H_c} d_c\sigma}$	−0.252733
δ_{Si}	−0.276789	δ_a	−0.266815	δ_c	−0.586952

The orthogonal ETB basis functions $\mathfrak{B}_{\text{final}}$ of Si, Ga, and As atoms are shown in Fig. 6. The ETB basis functions are slightly environment dependent because they are orthogonal. Thus, the ETB basis functions are not invariant under arbitrary rotations but invariant under symmetry operations within the T_d group, as pointed out by Slater and Koster [24]. It can be seen from Figs. 6(a) to 6(f) that the s and p orbitals show s and p features near the atom. More complicated patterns in the area farther away from the atom can be observed. These complicated patterns correspond to components with high angular momenta. The feature of an orthogonal ETB basis function resembles the augmented basis functions used in *ab initio* level calculations such as APWs and muffin-tin orbitals (MTOs). The orthogonal ETB basis functions have multiple angular parts in each orbital, as shown by Figs. 6(g)–6(i). The s-, p-, and d-type ETB basis functions are dominated by components with $l = 0, 1$, and 2, respectively. More than 90% of the s, p, and d orbitals are comprised of their $l = 0$, 1, and 2 components, respectively. The excited s^*-type ETB basis functions have higher angular momentum, and the $l = 0$ components have contributions of 60% to 70%. The second largest contribution in s^* orbitals is the f component with $l = 3$. The f component attached to the s^* orbitals has an angular part equivalent to real-space function xyz. This is a result of the existence of an xyz-like crystal field near each atom in zinc-blende and diamond structures.

B. Application to UTBs

To validate the transferability of the ETB model, band structures and eigenfunctions of [001] UTBs passivated by hydrogen atoms are calculated by both HSE06 and ETB models. The current calculations assume no strain in the UTBs. In the HSE06 calculations, charged hydrogen atoms are used to passivate the dangling bonds of the surface atoms in GaAs UTBs. The surface As and Ga atoms are passivated by charged hydrogen atoms with a 3/4 (denoted by H_{As}) and 5/4 (denoted by H_{Ga}) electron, respectively. The charged hydrogen atoms neutralize most of the surface-induced electric field in the UTBs. As a result, the charge distribution and local potential shows almost flat envelopes inside the UTBs. A small deviation in the potential can be observed only at the surface Si/Ga/As atoms. The nearly flat potential envelope

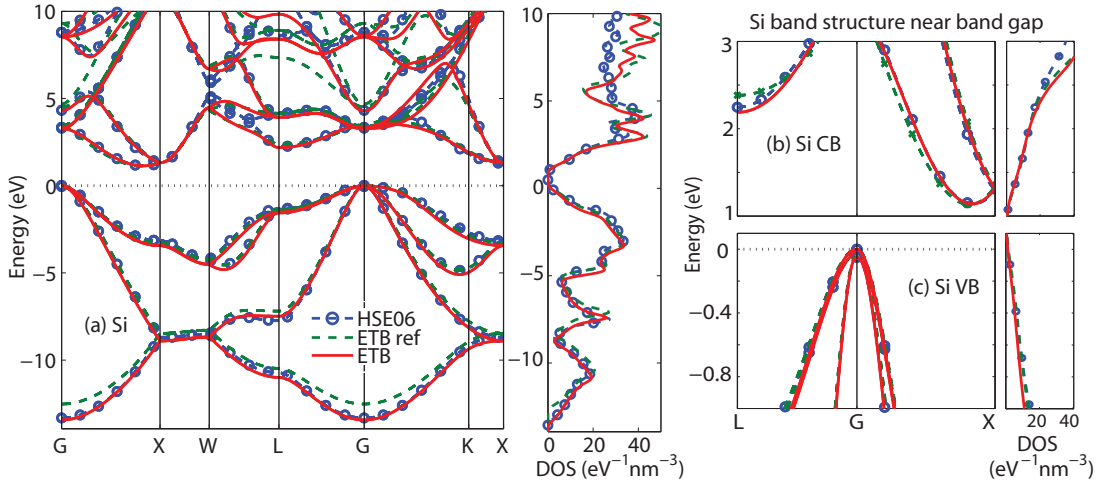

FIG. 4. (Color online) Band structure and density of states of bulk Si. ETB band structure agrees with (a) the HSE06 band structure, especially for (b) bottom conduction bands and (c) top valence bands.

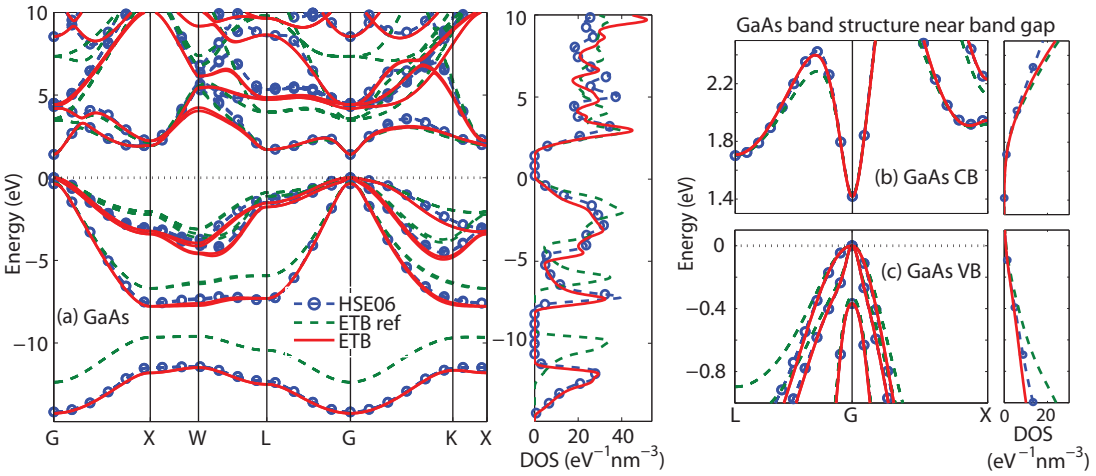

FIG. 5. (Color online) Band structure and density of states of bulk GaAs. ETB band structure agree with (a) the HSE06 band structure, especially for (b) bottom conduction bands and (c) top valence bands.

suggests geometry-dependent built-in potentials are needed only for surface atoms. Thus, the comparisons between self-consistent hybrid functional calculations and single-shot ETB calculations are fair.

The HSE06 calculations show that the hydrogen orbitals contribute to the deep valence bands; thus, hydrogen atoms are considered explicitly into the ETB Hamiltonian of UTBs in this work. The 1s orbital is used as the ETB basis function

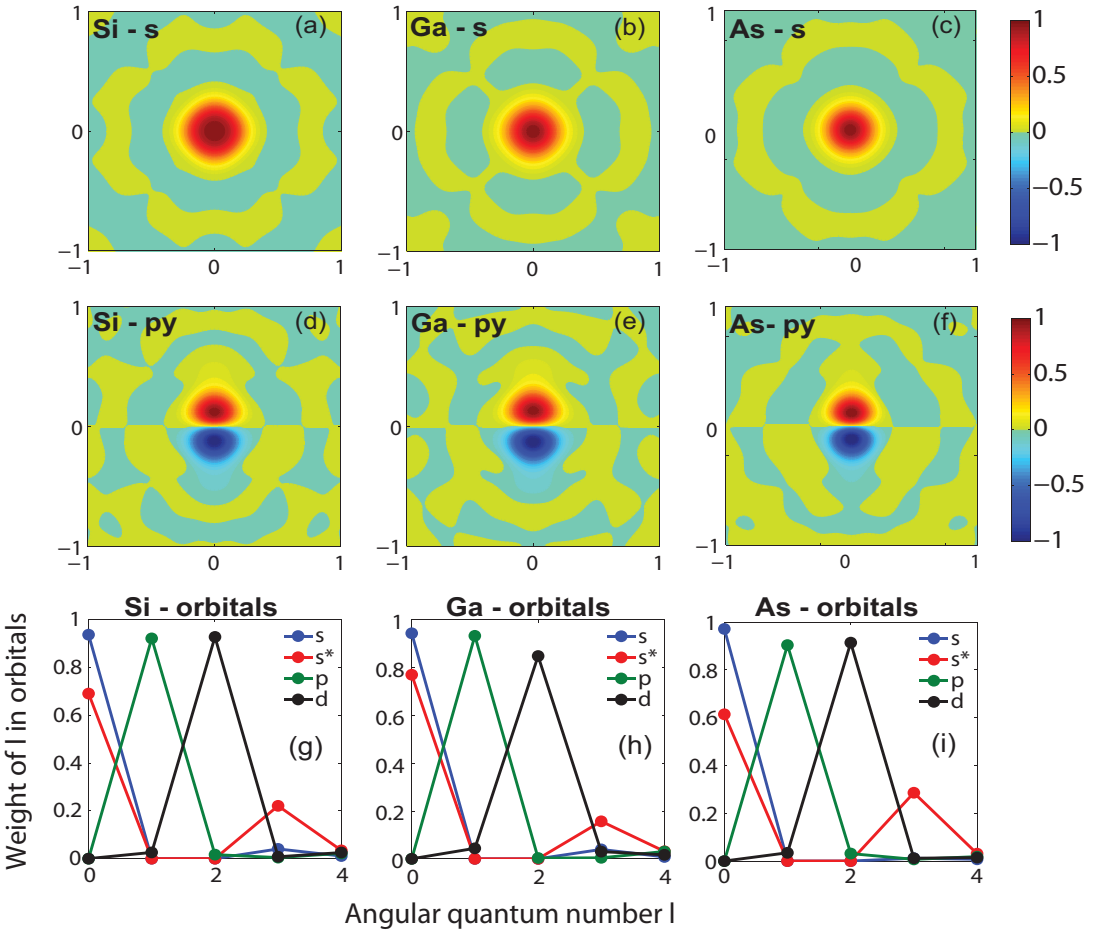

FIG. 6. (Color online) Contours of selected ETB basis functions of (a) and (d) Si, (b) and (e) Ga, and (c) and (f) As atoms. (top) The contours of s orbitals of Si, Ga, and As atoms in the x-y plane. (middle) The contours of p_y orbitals of Si, Ga, and As atoms. (bottom) The contribution of different angular momenta in basis functions of (g) Si, (h) Ga, and (i) As atoms. The ETB basis functions of Si and GaAs are highly localized basis functions with one dominant angular momentum.

for hydrogen atoms. The explicit-passivation model includes extra Slater-Koster-type ETB parameters for hydrogen and hydrogen bonds $E_{s_H s}$, $V_{s_H s\sigma}$, $V_{s_H p\sigma}$, $V_{s_H s^*\sigma}$, and $V_{s_H d\sigma}$. For the rest of the UTBs, the bulk Si/GaAs parameters listed in Table III are used. Furthermore, a geometry- and element-dependent potential δ is included for surface atoms. The on-site energies of the surface atoms are shifted by δ. The on-site energies of the surface Ga and As atoms thus become $E_{\alpha_c} + \delta_c$ and $E_{\alpha_a} + \delta_a$, respectively. Here α stands for s, p, d, and s^* orbitals. ETB parameters of Si/GaAs in Si/GaAs UTBs are identical to the parameters of unstrained bulk materials provided in Sec. III A. To determine the passivation parameters, an extra fitting process is needed: the band structure and wave functions of UTBs with 17 Si/GaAs atomic layers are considered. Targets considered in the fitting process include the direct and indirect band gaps of the UTBs and top valence and lowest conduction states and band structures from 0.5 eV below the top valence bands to 0.5 eV above the lowest conduction band.

To determine the ETB parameters of H passivation, band structures and real-space wave functions of selected bands near the Fermi level of the UTBs are considered as fitting targets. The inclusion of wave functions as targets serves the purpose of correcting possible problematic states. The target Si/GaAs UTBs contain 17 Si/GaAs atomic layers. Parameters for hydrogen atoms are also shown in Table III. In GaAs UTBs, As and Ga are passivated by hydrogen atoms with different charges; thus, the hydrogen atoms have different on-site energies when different types of atoms are passivated. The hydrogen atoms bonding with As atoms are charged positively, while the ones bonding with Ga atoms are charged negatively. Consequently, the H_c which forms a bond with As has a higher on-site energy than the H_a which forms a bond with Ga.

Band structures of Si/GaAs UTBs are shown in Fig. 7. The ETB band structures match the HSE06 band structures well for energies ranging from 1 eV below the topmost valence bands to 1 eV above the lowest conduction bands. Using the explicit ETB basis functions, ETB wave functions of UTBs with subatomic resolution are obtained and can be

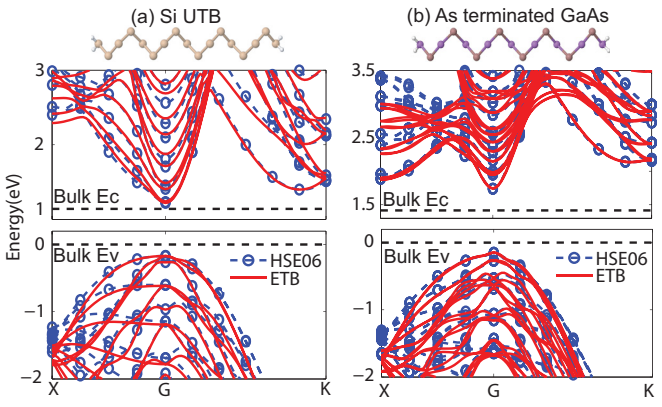

FIG. 7. (Color online) Band structures of 001 (a) Si and (b) As-terminated GaAs UTBs by ETB agree with HSE06 band structures, demonstrating the bulk Si and GaAs ETB parameters are transferable to UTB cases. All UTBs contain 17 Si/GaAs atomic layers (with thickness $4a_0$).

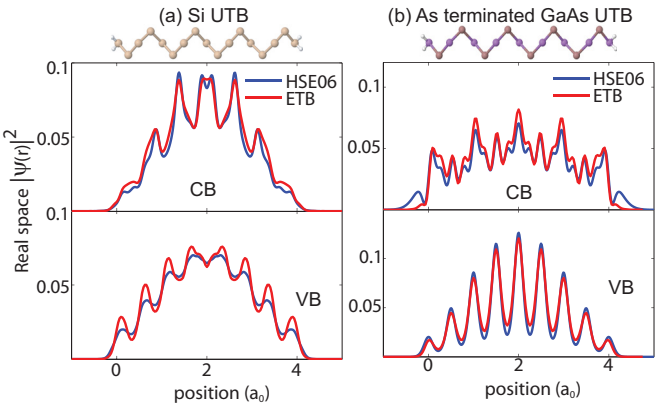

FIG. 8. (Color online) Planar averaged real-space probability amplitudes of the lowest conduction and topmost valance states of 001 (a) Si and (b) As-terminated GaAs UTBs by HSE06 and ETB calculations. With the real-space TB basis functions, the real-space probability amplitudes of TB calculations show reasonable agreement with the HSE06 probability amplitudes. UTBs contain 17 Si/GaAs atomic layers (with thickness $4a_0$).

compared with corresponding HSE06 wave functions. Planar averaged probability amplitudes of wave functions of the lowest conduction band and topmost valence bands in Si/GaAs UTBs are shown in Fig. 8. It can be seen that not only the envelope but also details of the subatomic resolution of the ETB planar averaged $|\psi|^2$ show agreement with corresponding HSE06 results. On the other hand, Fig. 9 compares the ETB atom-site-resolved probability amplitudes among ETB models in the present and previous works (Refs. [12,33]). The cations and anions in GaAs UTBs form different envelopes for all of the presented states. The lowest conduction and highest valence states turn out to be well-confined states in Si UTBs in all of the calculations. However, in GaAs UTBs, the lowest conduction states have a significant contribution from the surface atoms. In Si ETB probability amplitudes by parametrizations from Ref. [33] show similar envelopes compared to the ETB and HSE06 probability amplitudes in this work. Figure 9(d) shows the problematic valence states in As-terminated GaAs UTB from parameters from Ref. [12]. The corresponding valence states from this work turn out to be well-confined ones. To investigate this issue in more detail, in Fig. 10, ETB atom-site-resolved probability amplitudes for the topmost valence states of the four possible As-terminated GaAs UTBs are plotted: parameters from Ref. [12] and implicit passivation [13] [Fig. 10(a)], parameters from Ref. [12] and explicit passivation [Fig. 10(b)], parameters from this work and implicit passivation, and [Fig. 10(c)], and parameters from this and explicit passivation [Fig. 10(d)]. It is clear that, for a given set of bulk parameters, the implicit-passivation model leads to wave functions that are less confined than those of the explicit-passivation model. On the other hand, with the same passivation model, the ETB parameters from this work show more confined top valence states than the existing ETB parameters. Thus, the unconfined ETB state using the existing parameter set and the implicit-passivation model appears to be due to both the bulk GaAs parameters and the passivation model. The implicit model [13] replaces

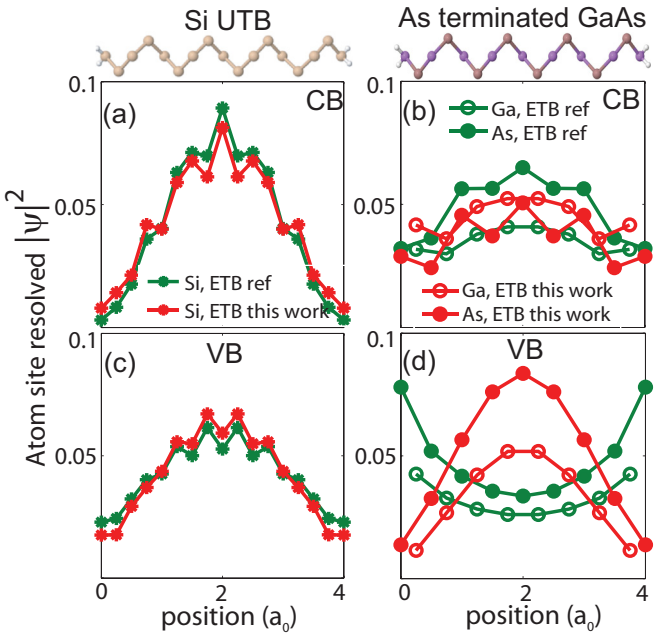

FIG. 9. (Color online) ETB atom-site-resolved probability amplitudes of (a) and (c) Si and (b) and (d) As-terminated GaAs UTBs using ETB parameters in this work and previous work [12,33]. The ETB atom site probability using different parameters is qualitatively similar in Si UTB, while the ETB atom site probability in As GaAs is more sensitive to the parameter sets and passivation models; that is, the valence states with parameters and passivation model from previous work are not confined. UTBs contain 17 atomic layers (thickness is $4a_0$).

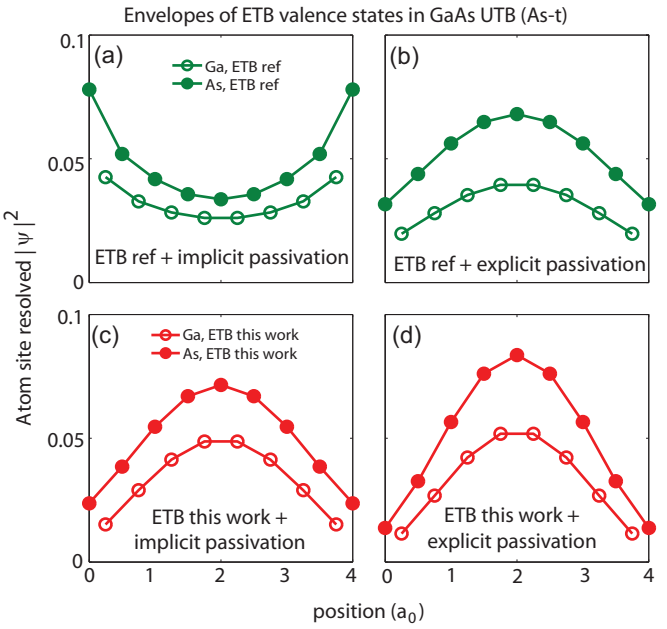

FIG. 10. (Color online) Comparison of ETB wave functions using different ETB parameters and passivation models. (a) and (b) use ETB parameters in Ref. [12]. (c) and (d) use ETB parameters in this work. (a) and (c) correspond to the implicit-passivation model [13]; (b) and (d) correspond to the explicit-passivation model. The ETB parameters with the explicit-passivation model show the most confined states, while the previous parameters and implicit-passivation model lead to less confined states.

the s and p orbitals of the surface atoms with sp^3 hybrids and raises the energy of the dangling hybrids by $\delta_{sp3} = 30$ eV. The d and s^* orbitals are left completely unpassivated, and the unconfined states of Fig. 10(a) are only slightly affected by changing the value of δ_{sp3}. The impact of changing the implicit-passivation model to the explicit-passivation model is obvious by comparing Fig. 10(a) to Fig. 10(b), as well as Fig. 10(c) to Fig. 10(d). To better understand the impact of bulk parameters on this behavior, the contribution of orbitals to the bulk bands by different parameter sets is compared. Obvious differences are found at the d-orbital contributions of the topmost bulk valence states at the Γ point. The bulk valence states from parameters from Ref. [12] have about a 16% contribution from the d orbital of Ga, while the ones from parameters from this work have only 8.5%. This discrepancy suggests either d-orbital on-site energies are excessively low or coupling of p_a and d_c is excessively strong in the parameter set from Ref. [12]. It turns out that the couplings of p_a and d_c are the major problematic parameters in the previous parameter set: by reducing the magnitude of the nearest-neighbor p_a-d_c coupling parameters in both sets as $V_{p_a d_c \sigma} \rightarrow V_{p_a d_c \sigma} + 0.3$ eV, $V_{p_a d_c \pi} \rightarrow V_{p_a d_c \pi} - 0.3$ eV, remarkably, in both cases the topmost valence-band state became much more confined. Bulk valence-band (VB) wave functions in the modified and original parameter sets tell the story: The general trend is that bulk sets which generate more p-like top-of-the-VB states give better confinement under passivation (especially implicit passivation) than those with higher d content. The reduction of $|V_{p_a d_c \sigma}|$ and $|V_{p_a d_c \pi}|$ leads to more p-like top-of-the-VB states. The Ga-terminated case has fewer passivation problems because its top-of-the-VB bulk states have a larger contribution from the As atoms than from the Ga atoms.

Figure 11 shows the band gaps of the Si and GaAs [001] UTBs as functions of UTB thickness. With the ETB parameters from this work, the ETB band gaps of Si and GaAs UTBs with thicknesses from 0.5 to 4 nm agree well with the gaps from HSE06 calculations. The ETB band gaps of Si UTBs using parameters from previous work also show good agreement with the HSE06 results. However, the ETB band gaps of GaAs UTBs using parameters from previous work and the implicit-passivation model are around 20% lower than the hybrid functional results. The gaps of GaAs UTBs terminated with Ga and As atoms are very close in value for both hybrid functional and ETB results in this work; however, the gaps of GaAs UTBs terminated with Ga and As atoms from previous parametrizations and the implicit-passivation model show 0.1 to 0.2 eV discrepancies. The band gap change in Si UTBs thicker than 3 nm can be model by the effective-mass model (assuming a parabolic E-k relation). However, in the GaAs UTBs, the discrepancies between effective-mass calculations and HSE06 or TB calculations are obvious for all GaAs UTBs presented, suggesting the nonparabolic feature of the GaAs valleys has a significant impact on GaAs nanostructures. The gaps from previous parameterization with the implicit-passivation model of As-terminated GaAs UTBs have lower confined energies due to the unconfined valence states.

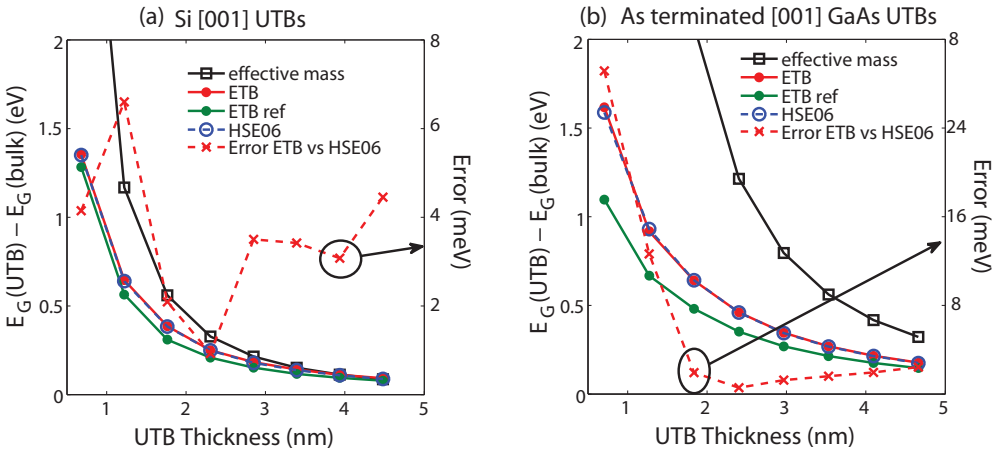

FIG. 11. (Color online) Band gaps of (a) Si UTBs and (b) As-terminated UTBs) by HSE06 and ETB calculations. For the presented UTBs with thickness ranging from 1 to 4.5 nm, the ETB band gaps have discrepancies of less than 10 meV compared with HSE06 ones. The band gap changes by the effective-mass calculation show agreement with HSE06 for Si UTBs thicker than 3 nm, while the effective-mass calculations have obvious discrepancies for all GaAs UTBs. The HSE06 and ETB calculations using parameters from this work consider hydrogen atoms explicitly, while the ETB calculations using parameters from previous work are based on the implicit-passivation model [13].

IV. CONCLUSION

It has been shown that the existing ETB parametrization together with the implicit-passivation model gives unphysical states in As-terminated GaAs UTB calculations. A more reliable technique of *ab initio* mapping which generates ETB parameters and basis functions *ab initio* is developed. The *ab initio* mapping process is applied to both bulk Si and GaAs. Slater-Koster-type ETB parameters within first-nearest-neighbor approximation and highly localized ETB basis functions are obtained. The ETB parameters and basis functions of Si and GaAs are validated in corresponding UTB systems with passivation models that consider hydrogen atoms explicitly. Band gaps in Si and GaAs UTBs with different thicknesses are also calculated by HSE06, ETB, and the effective-mass model. Compared with the existing ETB parametrizations and implicit-passivation model, the ETB calculations in this work show good agreement with HSE06 calculations in both band structures and wave functions. This work shows that the ETB parameters from *ab initio* mapping have good transferability. The mapping method developed here significantly reduces the uncertainty in both bulk and passivation models.

ACKNOWLEDGMENTS

This research was funded by Purdue University and the Semiconductor Research Corporation. The use of nanoHUB.org computational resources operated by the Network for Computational Nanotechnology funded by the US National Science Foundation under Grants No. EEC-0228390, No. EEC-1227110, No. EEC-0228390, No. EEC-0634750, No. OCI-0438246, No. OCI-0832623, and No. OCI-0721680 is gratefully acknowledged. M.P.'s work was supported by US National Science Foundation Nanoelectronics for 2020 and beyond under Grant No. MR05-20415. E. Wilson from Network for Computational Nanotechnology at Purdue University is acknowledged for improving the manuscript.

[1] Y. K. Choi, K. Asano, N. Lindert, V. Subramanian, T. J. King, J. Bokor, and C. Hu, IEEE Electron Device Lett. **21**, 254 (2000).
[2] D. Hisamoto, C. Lee, W, J. Kedzierski, H. Takeuchi, K. Asano, C. Kuo, E. Anderson, J. King, T, J. Bokor, and C. Hu, IEEE Electron Device Lett. **24**, 2320 (2000).
[3] J. Xiang, W. Lu, Y. Hu, Y. Wu, H. Yan, and C. M. Lieber, Nature (London) **441**, 489 (2006).
[4] R. Hatcher and C. Bowen, Appl. Phys. Lett. **103**, 162107 (2013).
[5] A. Krukau, O. Vydrov, A. Izmaylov, and G. Scuseria, J. Chem. Phys. **125**, 224106 (2006).
[6] M. S. Hybertsen and S. G. Louie, Phys. Rev. B **34**, 5390 (1986).
[7] S. Ismail-Beigi and S. G. Louie, Phys. Rev. Lett. **90**, 076401 (2003).
[8] J. Fonseca, T. Kubis, M. Povolotskyi, B. Novakovic, A. Ajoy, G. Hedge, H. Ilatikhameneh, Z. Jiang, P. Sengupta, Y. Tan *et al.*, J. Comput. Electron. **12**, 592 (2013).
[9] G. Klimeck, F. Oyafuso, T. B. Boykin, C. R. Bowen, and P. V. Allmen, Comput. Model. Eng. Sci. **3**, 601 (2002).
[10] R. Lake, G. Klimeck, and S. Datta, Phys. Rev. B **47**, 6427 (1993).
[11] J.-M. Jancu, R. Scholz, F. Beltram, and F. Bassani, Phys. Rev. B **57**, 6493 (1998).
[12] T. B. Boykin, G. Klimeck, R. C. Bowen, and F. Oyafuso, Phys. Rev. B **66**, 125207 (2002).
[13] S. Lee, F. Oyafuso, P. von Allmen, and G. Klimeck, Phys. Rev. B **69**, 045316 (2004).
[14] G. Kresse and J. Joubert, Phys. Rev. B **59**, 1758 (1999).
[15] M. C. Toroker, D. K. Kanan, N. Alidoust, L. Y. Isseroff, P. Liao, and E. A. Carter, Phys. Chem. Chem. Phys. **13**, 16644 (2011).
[16] C. Gong, G. Lee, B. Shan, E. M. Vogel, R. M. Wallace, and K. Cho, J. Appl. Phys. **108**, 123711 (2010).
[17] N. Marzari and D. Vanderbilt, Phys. Rev. B **56**, 12847 (1997).
[18] I. Souza, N. Marzari, and D. Vanderbilt, Phys. Rev. B **65**, 035109 (2001).

[19] X. Qian, J. Li, L. Qi, C.-Z. Wang, T.-L. Chan, Y.-X. Yao, K.-M. Ho, and S. Yip, Phys. Rev. B **78**, 245112 (2008).
[20] W. C. Lu, C. Z. Wang, T. L. Chan, K. Ruedenberg, and K. M. Ho, Phys. Rev. B **70**, 041101 (2004).
[21] A. Urban, M. Reese, M. Mrovec, C. Elsässer, and B. Meyer, Phys. Rev. B **84**, 155119 (2011).
[22] Y. Tan, M. Povolotskyi, T. Kubis, Y. He, Z. Jiang, G. Klimeck, and T. Boykin, J. Comput. Electron. **12**, 56 (2013).
[23] Z. Jiang, M. A. Kuroda, Y. Tan, D. M. Newns, M. Povolotskyi, T. B. Boykin, T. Kubis, G. Klimeck, and G. J. Martyna, Appl. Phys. Lett. **102**, 193501 (2013).
[24] J. C. Slater and G. F. Koster, Phys. Rev. **94**, 1498 (1954).
[25] A. V. Podolskiy and P. Vogl, Phys. Rev. B **69**, 233101 (2004).
[26] Y.-S. Kim, K. Hummer, and G. Kresse, Phys. Rev. B **80**, 035203 (2009).
[27] N. Ashcroft and N. Mermin, *Solid State Physics* (Saunders College, Philadelphia, 1976).
[28] P.-O. Lowdin, J. Chem. Phys. **18**, 365 (1950).
[29] L. Zeng, Y. He, M. Povolotskyi, X. Liu, G. Klimeck, and T. Kubis, J. Appl. Phys. **113**, 213707 (2013).
[30] G. Kresse and J. Furthmuller, Comput. Mater. Sci. **6**, 15 (1996).
[31] J. Heyd, G. Scuseria, and M. Ernzerhof, J. Chem. Phys. **124**, 219906 (2006).
[32] J. P. Perdew, K. Burke, and M. Ernzerhof, Phys. Rev. Lett. **77**, 3865 (1996).
[33] T. B. Boykin, G. Klimeck, and F. Oyafuso, Phys. Rev. B **69**, 115201 (2004).